INSTITUTE OF PHYSICS PUBLISHING NANOTECHNOLOGY
Nanotechnology **17** (2006) 2636–2640 doi:10.1088/0957-4484/17/10/032

ZnO nanoparticles embedded in sapphire fabricated by ion implantation and annealing

X Xiang[1], X T Zu[1,2,4], S Zhu[3], Q M Wei[3], C F Zhang[1], K Sun[3] and L M Wang[3]

[1] Department of Applied Physics, University of Electronic Science and Technology of China, Chengdu, 610054, People's Republic of China
[2] International Center for Material Physics, Chinese Academy of Sciences, Shenyang 110015, People's Republic of China
[3] Department of Nuclear Engineering and Radiological Sciences, University of Michigan, Ann Arbor, MI 48109-2104, USA

E-mail: xiaotaozu@yahoo.com

Received 16 February 2006, in final form 22 March 2006
Published 5 May 2006
Online at stacks.iop.org/Nano/17/2636

Abstract
ZnO nanoparticles were fabricated in sapphire (α-Al_2O_3 single crystal) by Zn ion implantation (48 keV) at an ion fluence of 1×10^{17} cm^{-2} and subsequent thermal annealing in a flowing oxygen atmosphere. Transmission electron microscopy (TEM) analysis revealed that metallic Zn nanoparticles of 3–10 nm in dimensions formed in the as-implanted sample and that ZnO nanoparticles of 10–12 nm in dimensions formed after annealing at 600 °C. A broad absorption band, peaked at 280 nm, appeared in the as-implanted crystal, due to surface plasma resonance (SPR) absorption of metallic Zn nanoparticles. After annealing at 600 °C, ZnO nanoparticles resulted in an exciton absorption peak at 360 nm. The photoluminescence (PL) of the as-implanted sample was very weak when using a He–Cd 325 nm line as the excitation source. However, two emission peaks appeared in the PL spectrum of ZnO nanopraticles, i.e., one ultraviolet (UV) peak at 370 nm and the other a green peak at 500 nm. The emission at 500 nm is stronger and has potential applications in green/blue light-emitting devices.

1. Introduction

Metallic clusters embedded in an insulating host were among the first nanocomposite systems to be formed by ion implantation. It has attracted extensive investigation because of pronounced optical effects, including surface plasmon resonance (SPR) absorption and strong third-order nonlinear optical (NLO) susceptibility [1]. Recently, oxide nanoparticles have been drawing much attention because of their peculiar optical properties, such as NiO, CuO, Cu_2O, and VO_2 in silica glasses SiO_2 and sapphire [2–5]. ZnO is well known as a versatile wide band gap (∼3.3 eV) semiconducting material with a large exciton binding energy of 60 meV, which allows excitonic recombination and optically pumped laser oscillations even at room temperature [6]. Following the demonstration of blue-green light emitting diodes (LEDs) and lasers using II–VI compounds, ZnO has been intensively studied for optoelectric applications in both the visible and ultraviolet (UV) regions. Ion implantation has become a versatile and powerful technique for forming nanoparticles. ZnO nanoparticles with strong exciton photoluminescence (PL) have been prepared in silica glasses (SiO_2) and CaF_2 single crystals by ion implantation and subsequent thermal annealing [7–11]. Sapphire (α-Al_2O_3) is a good candidate to allow the controlled formation of colloidal dispersions of precipitates using ion implantation, due to its high chemical and thermal stability. Up to now, there has been no report about the embedded Zn/ZnO nanopartilces fabricated in sapphire. In this work, we fabricated Zn and ZnO nanoparticles embedded in α-Al_2O_3 single crystals by ion implantation

[4] Author to whom any correspondence should be addressed.

with or without subsequent thermal annealing. These ZnO nanoparticles have strong visible photoluminescence. Transmission electron microscopy (TEM), optical absorption, and photoluminescence spectroscopy have been utilized to characterize the microstructure and optical properties of embedded Zn/ZnO nanoparticles, respectively.

2. Experimental details

Optical polished (0001) α-Al_2O_3 single crystals (sapphire), 10 mm × 10 mm × 0.5 mm in dimensions, were implanted with Zn ions of 48 keV up to a fluence of 1×10^{17} cm^{-2} in a vacuum chamber of 1.8×10^{-3} Pa. The samples were kept at room temperature with the circulation of cooling water during ion implantation. The ion current density was limited to less than 5 μA cm^{-2} to avoid overheating the samples. The samples were tilted off-axis by about 7° to avoid channelling implantation. After implantation, all the crystals turned gray and their transparency decreased. The as-implanted samples were annealed for 1 h in a quartz tube furnace at temperatures between 300 °C and 900 °C in increments of 100 °C under a flowing O_2 atmosphere. The heating rate was controlled at 10 °C min^{-1}.

Optical absorption measurements in the UV–visible range were made in a SHIMADZU UV-2550 spectrophotometer at room temperature, with a deuterium lamp for UV and a tungsten halogen lamp for the visible region. The wavelength used in the experiment ranged from 200 to 800 nm. A JEM 2010F field emission gun electron microscope operating at 200 keV was used for bright-field TEM, selected-area electron diffraction (SAED) and high-resolution electron microscopy (HREM). TEM samples were prepared in cross-section to allow observation of the depth distribution of nanoparticles and radiation damage [12]. Room-temperature photoluminescence (PL) was excited by the 325 nm line (3.81 eV) from a Kimmon He–Cd laser with an excitation power of 65 mW. The spectra were detected by a SPEX 1403 double grating monochromator and a CCD array.

3. Results and discussion

The optical absorption spectra of the as-received, as-implanted and annealed α-Al_2O_3 single crystals are shown in figure 1. The spectra have been shifted vertically to avoid overlapping, except that of the as-received sample. The absorption around 200 nm exists in all the spectra, which is the inherent absorption of the purchased α-Al_2O_3 single crystals. After Zn^+ ion implantation at a fluence of 1×10^{17} cm^{-2}, a clear and broad absorption peak appears at ∼280 nm. This absorption peak is attributed to surface plasma resonance (SPR) absorption of metallic Zn nanoparticles. Actually, similar absorption peaks have been observed at 234–259 nm in SiO_2 glasses and at 295 nm in MgO single crystals [7–10, 13]. The absorption peak shifted slightly towards the longer wavelength due to the growth of nanoparticles with increasing annealing temperature. The spectrum of annealed sample at 500 °C is a transition spectrum, because it includes both the absorption peak of Zn nanoparticles and the absorption edge of ZnO nanoparticles. After annealing at 600 °C for 1 h, the SPR absorption peak disappears and a clear absorption peak appears at ∼360 nm,

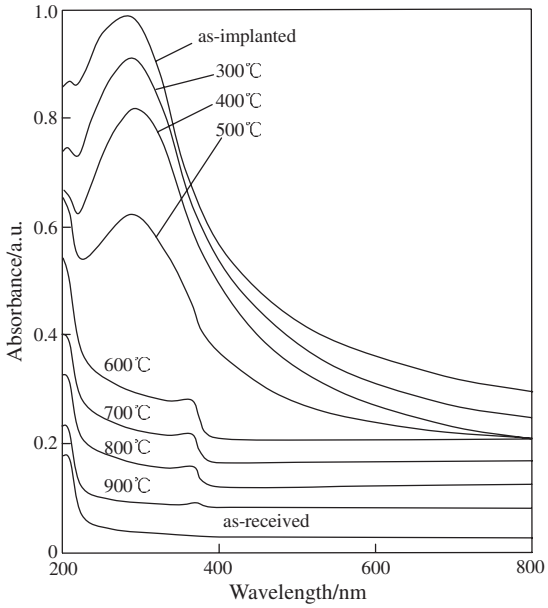

Figure 1. Optical absorption spectra of as-received, as-implanted and annealed α-Al_2O_3 single crystals at different temperatures.

which is consistent with the exciton absorption of ZnO [7–11]. The intensity of this exciton absorption peak decreases with a further increase in annealing temperature. Apparently, this intensity decrease does not indicate a decrease of Zn content in the sample. This may be due to the decreased concentration of ZnO nanoparticles, because of the formation of $ZnAl_2O_4$ spinel during thermal annealing in O_2 atmosphere [14]. The microscopic morphology of Zn and ZnO nanoparticles has been characterized by TEM imaging with the main results shown below.

Figure 2 shows a cross-sectional bright-field TEM image (a) and a high-resolution TEM (HREM) image (b) of Zn nanoparticles embedded in α-Al_2O_3 formed by Zn^+ ion implantation at a dose of 1×10^{17} cm^{-2}. Nearly spherical embedded Zn nanoparticles of 3–10 nm in diameter are observed and the ion-implanted area is amorphized, which is consistent with Ni^+ ion-implanted α-Al_2O_3 [15]. The Zn nanoparticles distribute in a range about 15–45 nm below the surface, which is consistent with the calculated result by TRIM 96 (the maximum concentration of 5×10^{22} Zn^+ cm^{-3} at ∼22 nm) without the consideration of volume swelling due to the implanted ions [16]. According to the simulation of TRIM code and the measurement of RBS (Rutherford backscattering spectrometry), the implanted ions show a Gaussian distribution. A series of investigations have been used to find out how to confine the implanted ions in a narrow layer. The methods include generating chemical barriers, engineering defect barriers on both sides of the implanted layer, as well as combining two nonequilibrium processes, ion implantation and post-implantation irradiation [17, 18]. In general, the ion implantation techniques used to form nanoclusters may be categorized as follows [1, 17]: (1) room-temperature implantation followed by high-temperature annealing; (2) room-temperature implantation at a dosage above the threshold dose for spontaneous nanocrystals formation; (3) ion implantation at elevated temperatures. In this study, Zn nanoparticle formation is by

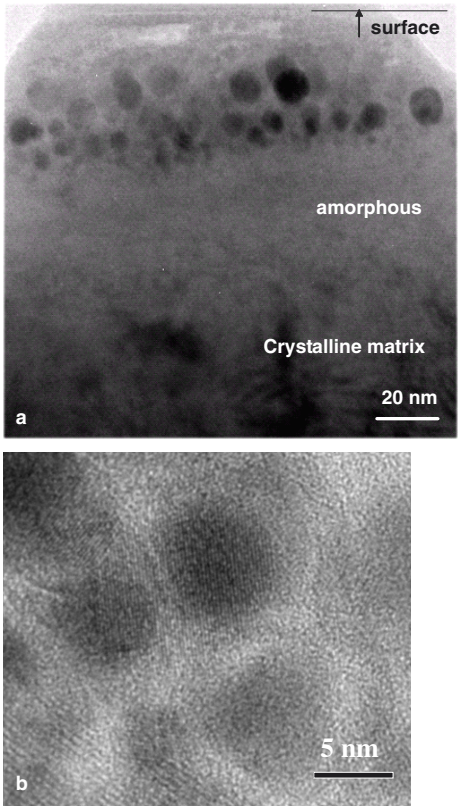

Figure 2. A cross-sectional bright-field TEM image (a) and a high-resolution TEM image (b) of Zn nanoparticles embedded in Al_2O_3 matrix.

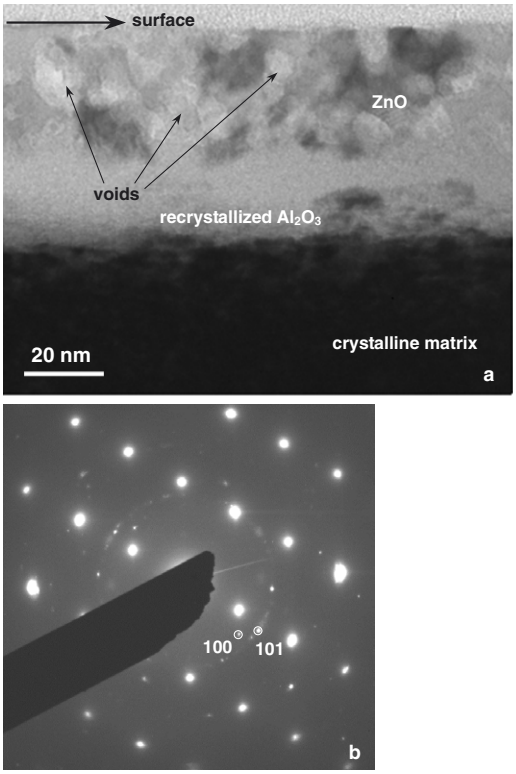

Figure 3. A cross-sectional bright-field TEM image (a) and a selected-area electron diffraction pattern (b) of ZnO nanoparticles embedded in Al_2O_3 matrix.

means of the second of the above. At room temperature, the ion fluence of 1×10^{17} cm^{-2} certainly leads to a local Zn concentration far above the solubility limit of Zn in Al_2O_3, thus the implanted Zn precipitate out. This is because the free energy of the system may be minimized by movement from the separation of metal into colloidal precipitates, i.e., large numbers of free metal ions tend to aggregate, precipitate, and form nanocrystals [19].

Figure 3 contains a cross-sectional bright-field TEM image (a) and a selected-area electron diffraction (SAED) pattern (b) of ZnO nanoparticles embedded in α-Al_2O_3 formed after annealing at 600 °C. The ZnO can be confirmed by the SAED pattern. Figure 4 is a high-resolution TEM image of ZnO nanoparticles, showing the nanoparticles of 10–12 nm in dimensions. The moiré fringes indicate the precipitation of ZnO nanoparticles after annealing. It is clear that the ZnO nanoparticles formed close to the surface of the α-Al_2O_3 single crystal, with a depth shallower than the projectile range of implanted Zn atoms. This indicates that the Zn atoms migrated towards the surface of the crystal during annealing in the oxygen atmosphere. At the same time, some high densities of large voids (labelled in figure 3(a)) are observed in the near-surface region due to the migration and precipitation of irradiation-induced vacancies. In the previous studies, multilayer structures were observed in the cross-sectional TEM images of the Zn^+-ion-implanted and subsequently annealed SiO_2. In detail, Liu *et al* observed three clear zones, i.e., a ZnO layer with particles of about 90×90 nm^2, a Zn-implanted silica layer, and a silica substrate [9]. Amekura *et al* observed

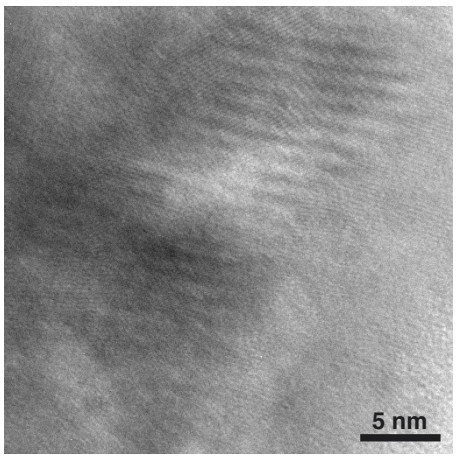

Figure 4. A high-resolution TEM image of ZnO nanoparticles in Al_2O_3 matrix.

four clear zones: droplet-like ZnO nanoparticles larger than 30 nm in diameter on the surface, nanoparticles of ∼5 nm in diameter in the shallower region, nanoparticles of ∼10 nm in diameter in the deeper region, and silica substrate. However, there are only two zones in the α-Al_2O_3 single crystal, i.e., a ZnO layer and a sapphire substrate. The difference may result from the two very different substrates. i.e., SiO_2 is amorphous and sapphire is crystalline. After annealing, the amorphous Al_2O_3 begins to recrystallize first at the interface of the amorphous and crystalline zones (labelled in figure 3(a)). The recrystallized Al_2O_3 grains have a different orientation

Table 1. PL of ZnO nanoparticles embedded in several insulator matrices.

Matrix	Annealing	PL peaks (nm)		Intensity ratio of green to UV (≈)	Reference
SiO_2	700 °C 1 h	375	500	1:2	[7]
	700 °C 2 h	377	500	1:7	[9]
CaF_2	400 °C 45 min	384	500	2:1	
	500 °C 45 min	372	—	—	[11]
	700 °C 45 min	379	—	—	
Al_2O_3	600 °C 1 h	370	500	3:1	This study

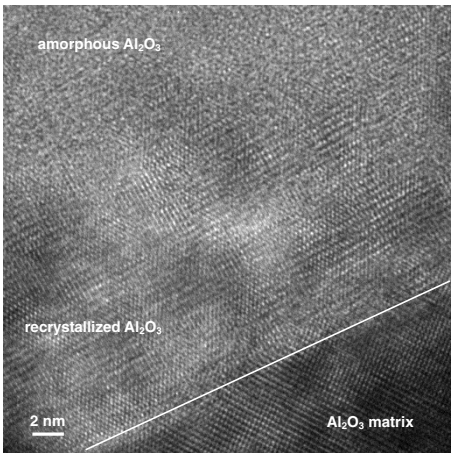

Figure 5. A high-resolution TEM image showing the recrystallized Al_2O_3 with different orientation relation with the matrix.

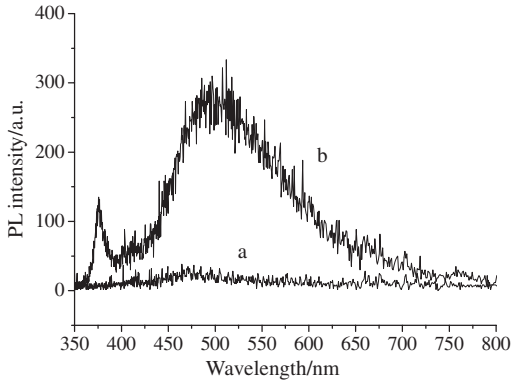

Figure 6. Photoluminescence spectra of the as-implanted (a) and the annealed (b) crystal at 600 °C at room temperature.

relationship with the original matrix, which can be observed in figure 5. However, the recrystallization was not complete after annealing at 600 °C for 1 h. The front surface area (labelled in figure 5) remained amorphous. Apparently, longer annealing time or higher annealing temperatures are needed to complete the recrystallization.

Figure 6 shows the photoluminescence (PL) spectra of the as-implanted crystal and the annealed crystal at 600 °C using He–Cd laser excitation at 325 nm at room temperature. There is a very weak PL band peaked at ∼470 nm in the as-implanted crystal. This may be due to the photoluminescence combination of both F (PL at 3.0 eV) and F_2 (PL at 2.4 eV) centres coexisting in Al_2O_3 induced by ion implantation [20]. The PL spectrum of the annealed crystal shows two PL peaks, one at 370 nm and the other at 500 nm, which have been observed in Zn^+-ion-implanted SiO_2 [7, 9]. The UV emission is the characteristic PL peak ascribed to ZnO free-exciton recombination at room temperature, which confirms the formation of ZnO nanoparicles after thermal annealing. This is because ZnO is a wide band gap semiconducting material with a large exciton binding energy of 60 meV, which allows excitonic recombination and optically pumped laser oscillations even at room temperature. The UV PL peak with a full width at half maximum (FWHM) of 11.5 nm (100 meV) is comparable to the high-purity ZnO grown by plasma-assisted MBE [21] and the ZnO nanoparticles in SiO_2 [7, 9], indicating good crystallinity of ZnO nanoparticles in this study. According to the previous studies, the green emission at ∼500 nm may originate from the deep levels [22, 23]. The deep-level emission at around 2.5 eV is associated with either surface state emission or excess Zn interstitials (or oxygen vacancies).

Up to now, both UV and green PL peaks of embedded ZnO nanoparitlces have been observed in SiO_2, CaF_2 and Al_2O_3 matrices by ion implantation and thermal annealing (listed in table 1). These PL spectra are similar to those of ZnO nanowires and nanorods [24]. Among them, the spectrum of the ZnO nanoparticles in Al_2O_3 is the most like those of ZnO nanowires and nanorods, and its intensity ratio of green to UV emission is highest. Furthermore, it was reported that the oxygen vacancies responsible for the green emission are located at the surface [22, 23]. Huang *et al* have reported the progressive increase of green light emission intensity relative to UV emission as the wire diameter decreases, which suggests that there is an increasing fraction of oxygen vacancies in the nanowires [25]. Dijken *et al* have also confirmed an increase in the visible emission intensity as the size of the ZnO particles decreases [26]. Therefore, the ratio of green to UV emission is dependent on the ZnO nanostructure's size. Consequently, the fact that the ZnO nanoparticles in Al_2O_3 have a higher ratio of green to UV emission than those in SiO_2 and CaF_2 should result from their smaller sizes. The green emission has potential applications in green/blue light-emitting devices.

4. Conclusion

ZnO nanoparticles were fabricated in α-Al_2O_3 single crystal by Zn ion implantation and subsequent thermal annealing in an O_2 atmosphere. TEM analysis revealed metallic Zn nanoparticles of 3–10 nm in the as-implanted sample and ZnO nanoparticles of 10–12 nm after annealing at 600 °C. A new broad absorption band, peaked at 280 nm, appeared in the

as-implanted crystal, due to SPR absorption of metallic Zn nanoparticles. After annealing at 600 °C, ZnO nanoparticles caused an exciton absorption peak at 360 nm. Two emission peaks appeared in the PL spectrum of ZnO nanopraticles, i.e., one UV peak at 370 nm and the other green peak at 500 nm. The green emission is stronger and has potential applications in green/blue light-emitting devices.

Acknowledgments

This study was supported financially by the NSAF Joint Foundation of China (10376006) and by the US Department of Energy under Grant DF-FG02-02ER46005 and by the Program for New Century Excellent Talents in University (NCET-04-0899) and by the PhD Funding Support Program of the Education Ministry of China (20050614013).

References

[1] Meldrum A, Haglund R F Jr, Boatner L A and White C W 2001 *Adv. Mater.* **13** 1431
[2] Amekura H, Umeda N, Takeda Y, Lu J and Kishimoto N 2004 *Appl. Phys. Lett.* **85** 1015
[3] Ikeyama M, Nakao S and Tazawa M 2002 *Surf. Coat. Technol.* **158/159** 720
[4] Nakao S, Wang S X, Wang L M, Ikeyama M, Miyagawa Y and Miyagawa S 2001 *Nucl. Instrum. Methods Phys. Res.* B **175–177** 202
[5] Lopez R, Boatner L A, Haynes T E, Feldman L C and Haglund R F Jr 2002 *J. Appl. Phys.* **92** 4031
[6] Bagnall D M, Chen Y F, Zhu Z, Yao T, Koyama S, Shen M Y and Goto T 1997 *Appl. Phys. Lett.* **70** 2230
[7] Amekura H, Umeda N, Sakuma Y, Kishimoto N and Buchal Ch 2005 *Appl. Phys. Lett.* **87** 013109
[8] Lee J K, Tewell C R, Schulze R K, Nastasi M, Hamby D W, Lucca D A, Jung H S and Hong K S 2005 *Appl. Phys. Lett.* **86** 183111
[9] Liu Y X, Liu Y C, Shao C L and Mu R 2004 *J. Phys. D: Appl. Phys.* **37** 3025
[10] Chen J, Mu R, Ueda A, Wu M H, Tung Y-S, Gu Z, Henderson D O, White C W, Budai J D and Zuhr R A 1998 *J. Vac. Sci. Technol.* A **16** 1409
[11] Liu Y C, Xu H Y, Mu R, Henderson D O, Lu Y M, Zhang J Y, Shen D Z, Fan X W and White C W 2003 *Appl. Phys. Lett.* **83** 1210
[12] Wang L M 1998 *Nucl. Instrum. Methods* B **312** 141
[13] van Huis M A, van Veen A, Schut H, Kooi B J, De Hosson J Th M, Du X S, Hibma T and Fromknecht R 2004 *Nucl. Instrum. Methods Phys. Res.* B **216** 390
[14] White C W, Meldrum A, Sonder E, Budai J D, Zuhr R A, Withrow S P and Henderson D O 1999 *Mater. Res. Soc. Symp. Proc.* **540** 219
[15] Xiang X, Zu X T, Zhu S and Wang L M 2004 *Appl. Phys. Lett.* **84** 52
[16] Ziegler J F, Biersack J P and Littmark U 1985 *The Stopping and Range of Ions in Solids* (New York: Pergamon)
[17] Ila D, Williams E K, Zimmerman R L, Poker D B and Hensley D K 2000 *Nucl. Instrum. Methods* B **166/167** 845
[18] Ila D, Williams E K, Smith C C, Poker D B, Hensley D K, Klatt C and Kalbitzer S 1999 *Nucl. Instrum. Methods* B **148** 1012
[19] Townsend P D 1987 *Rep. Prog. Phys.* **50** 501
[20] Kotomin E A and Popov A I 1998 *Nucl. Instrum. Methods Phys. Res.* B **141** 1
[21] Chen Y, Bagnall D M, Koh H J, Park K T, Hiraga K, Zhu Z and Yao T 1998 *J. Appl. Phys.* **84** 3912
[22] Zhao Q, Xu X Y, Song X F, Zhang X Z, Yu D P, Li C P and Guo L 2006 *Appl. Phys. Lett.* **88** 033102
[23] Zhang D H, Wang Q P and Xue Z Y 2003 *Appl. Surf. Sci.* **207** 20
[24] Wang R C, Liu C P, Huang J L and Chen S-J 2005 *Appl. Phys. Lett.* **86** 251104
[25] Huang M H, Wu Y Y, Feick H, Tran N, Weber E and Yang P 2001 *Adv. Mater.* **13** 113
[26] van Dijken A, Meulenkamp E A, Vanmaekelbergh D and Meijerink A 2000 *J. Lumin.* **87–89** 454